JPE 19-2-22

https://doi.org/10.6113/JPE.2019.19.2.569
ISSN(Print): 1598-2092 / ISSN(Online): 2093-4718

SSCI Mitigation of Series-compensated DFIG Wind Power Plants with Robust Sliding Mode Controller using Feedback Linearization

Penghan Li*, Linyun Xiong*, Jie Wang†, Meiling Ma*, and Muhammad Waseem Khan*

†,*School of Electronic Information and Electrical Engineering, Shanghai Jiao Tong University, Shanghai, China

Abstract

A robust controller is designed based on feedback linearization and sliding mode control to damp sub-synchronous control interaction (SSCI) in doubly fed induction generator (DFIG) wind power plants (WPPs) interfaced with the grid. A feedback-linearized sliding mode controller (FLSMC) is developed for the rotor-side converter (RSC) through feedback linearization, design of the sliding mode controller, and parameter tuning with the use of particle swarm optimization. A series-compensated 100-MW DFIG WPP is adopted in simulation to evaluate the effectiveness of the designed FLSMC at different compensation degrees and wind speeds. The performance of the designed controller in damping SSCI is compared with proportional-integral controller and conventional sub-synchronous resonance damping controller. Besides the better damping capability, the proposed FLSMC enhances robustness of the system under parameter variations.

Key words: Feedback linearization, PSO, Sliding mode control, SSCI, Wind power plant

I. INTRODUCTION

Sub-synchronous resonance (SSR) of wind power plants (WPPs) is a condition where wind turbines exchange energy with the grid at one or more natural frequencies below the fundamental frequency of the system [1], [2]. A new type of SSR called sub-synchronous control interaction (SSCI) has been identified in recent years [3], [4]. Studies have demonstrated that doubly fed induction generator (DFIG) WPPs are susceptible to SSCI due to fast-acting converter control [5]-[10].

Several control methods using flexible AC transmission systems have been proposed to mitigate SSR (or SSCI) in power systems, such as unified power flow controllers [11], static synchronous compensators [12], and thyristor-controlled series compensators [13]. Modification of existing controller is another option for damping SSCI. To stabilize the SSR of practical power systems, a combined control strategy composed of an excitation damping control and a generator terminal damping control was proposed [14]. With the derivative of the rotor speed deviation as the control input, a fuzzy logic control strategy was developed to damp SSR [15]. An adaptive controller was used for supplementary control to alleviate SSCI in DFIG WPPs [16]. A fuzzy based adaptive control strategy was proposed for the grid-side converters (GSC) and rotor-side converters (RSC) of DFIG to alleviate SSCI [17]. A parallel damping control strategy was proposed using the rotor torque analysis method [18]. The issue of SSCI was addressed by embedding suppression filters into the converter controller of a DFIG [19]. A filter-less damping control method was proposed for DFIG WPPs to alleviate SSCI [20]. However, the nonlinear dynamics of DFIGs was not considered in previous works' design procedures. Therefore, a nonlinear controller is developed in the current study to transcend the limitation of linear control schemes.

The feedback linearization (FL) method retains the nonlinearity through nonlinear feedback and coordinate transformation. Transformed systems are independent of predefined operations [21]. This characteristic is suitable for highly nonlinear DFIGs. However, a system under FL control could be sensitive to parameter variations. Sliding mode control (SMC) has been widely used to improve robust properties [22]. A high-order

Manuscript received Jun. 22, 2018; accepted Dec. 21, 2018
Recommended for publication by Associate Editor Zheng Wang.
†Corresponding Author: jiewangxh@sjtu.edu.cn
Tel: +86-13524666398, Shanghai Jiao Tong University
*Sch. Electron. Informat. Electr. Eng., Shanghai Jiao Tong Univ., China

SMC was designed for grid synchronization and power optimization of wind farms [23]. For DFIG-based WPPs, a fractional-order SMC was developed for maximum power point tracking [24]. An SMC was developed for GSC of DFIG to damp SSCI [25]. However, the power rating of GSC is only 25% of gerarator rating, which limits the effectiveness of the control method. Moreover, the impact of the number of online wind turbines (WTs) was neglected in [25], and the configuration of realistic WPPs was not considered in electromagnetic transient (EMT) simulation in [25]. Therefore, in the present work, a sliding mode controller is developed for RSC based on feedback linearization to damp SSCI at different compensation degrees, wind speeds, and number of online WTs. The design procedures of the proposed controller include feedback linearization, design of the sliding mode controller, and parameter tuning with use of particle swarm optimization (PSO). Eigenvalue analysis and EMT simulation based on a realistic WPP are performed to evalute the effectiveness of the proposed control method.

The remainder of this paper is organized as follows. The model of the DFIG WPP is presented in Section II. In Section III, the system is feedback linearized. In Section IV, the sliding mode controller for RSC is developed, and PSO is utilized for parameter tuning. In Section V, the effectiveness of the designed FLSMC is tested and compared with that of the PI controller and SSRDC at different compensation degrees and wind speeds. Concluding remarks are presented in Section VI.

II. System Model

As shown in Fig. 1, a 100 MW DFIG WPP is interfaced with series-compensated transmissions [10]. The WPP is an aggregation of 50 wind turbines, each with 2 MW power rating [25]. System data are presented in the Appendix.

The studied system includes the induction generator, shaft system, and BtB converter [10]. Shaft dynamics is expressed as follows:

$$\begin{cases} \dfrac{\mathrm{d}}{\mathrm{d}t}\omega_m = \dfrac{1}{2H_t}\left(T_{ae} - K_s\gamma - D_t\omega_m\right) \\ \dfrac{\mathrm{d}}{\mathrm{d}t}\omega_r = \dfrac{1}{2H_g}\left(K_s\gamma - D_g\omega_r - T_e\right) \\ \dfrac{\mathrm{d}}{\mathrm{d}t}\gamma = 2\pi f\left(\omega_m - \dfrac{\omega_r}{N_g}\right) \end{cases}, \tag{1}$$

where ω_r and ω_m are rotor angular frequency and rotor shaft angular frequency, respectively; T_{ae} and T_e are aerodynamic torque and electromagnetic torque, respectively; γ denotes the torsion angle; D denotes the torsion damping coefficient; H represents the inertia constant; K_s represents the torsion stiffness coefficient; N_g represents the gear ratio.

The electrical dynamics of the system is obtained by using Kirchhoff's current law and Kirchhoff's voltage law, which

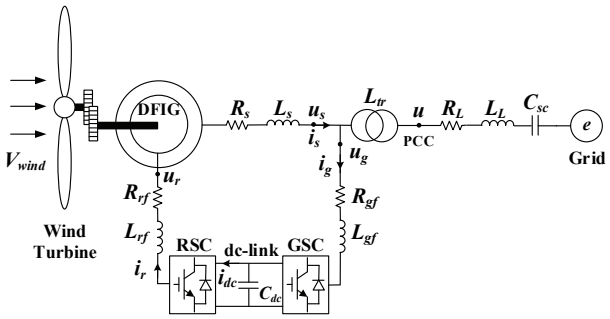

Fig. 1. DFIG-based WPP interfaced with the grid.

are expressed as follows:

$$\begin{cases} \dfrac{\mathrm{d}}{\mathrm{d}t}i_{rq} = -\omega_1 i_{rd} - \dfrac{R_{rf}}{L_{rf}}i_{rq} - \dfrac{u_{rq}}{L_{rf}} + \dfrac{u_{dc}}{L_{rf}}S_{rq} \\ \dfrac{\mathrm{d}}{\mathrm{d}t}i_{rd} = \omega_1 i_{rq} - \dfrac{R_{rf}}{L_{rf}}i_{rd} - \dfrac{u_{rd}}{L_{rf}} + \dfrac{u_{dc}}{L_{rf}}S_{rd} \end{cases}, \tag{2}$$

$$\frac{\mathrm{d}}{\mathrm{d}t}u_{dc} = \frac{1}{C_{dc}}i_{dc} - \frac{1}{C_{dc}}i_{rd}S_{rd} - \frac{1}{C_{dc}}i_{rq}S_{rq}. \tag{3}$$

$$\begin{cases} \dfrac{\mathrm{d}}{\mathrm{d}t}i_{sq} = -\omega_1 i_{sd} + \dfrac{R_s}{L_s}i_{sq} + \dfrac{u_{sq}}{L_s} \\ \dfrac{\mathrm{d}}{\mathrm{d}t}i_{sd} = \omega_1 i_{sq} + \dfrac{R_s}{L_s}i_{sd} + \dfrac{u_{sd}}{L_s} \end{cases}, \tag{4}$$

$$\begin{cases} \dfrac{\mathrm{d}}{\mathrm{d}t}i_{gq} = \omega_1 i_{gd} - \dfrac{R_{gf}}{L_{gf}}i_{gq} - \dfrac{u_{gq}}{L_{gf}} \\ \dfrac{\mathrm{d}}{\mathrm{d}t}i_{gd} = -\omega_1 i_{gq} - \dfrac{R_{gf}}{L_{gf}}i_{gd} - \dfrac{u_{gd}}{L_{gf}} \end{cases}, \tag{5}$$

$$\begin{cases} \dfrac{\mathrm{d}}{\mathrm{d}t}i_q = -\omega_1 i_d + \dfrac{R_L}{L_L}i_q + \dfrac{1}{L_L}\left(u_q - u_{scq} - e_q\right) \\ \dfrac{\mathrm{d}}{\mathrm{d}t}i_d = \omega_1 i_q + \dfrac{R_L}{L_L}i_d + \dfrac{1}{L_L}\left(u_d - u_{scd} - e_d\right) \end{cases}, \tag{6}$$

$$\begin{cases} \dfrac{\mathrm{d}}{\mathrm{d}t}u_{scq} = -\omega_1 u_{scd} + \dfrac{i_q}{C_{sc}} \\ \dfrac{\mathrm{d}}{\mathrm{d}t}u_{scd} = \omega_1 u_{scq} + \dfrac{i_d}{C_{sc}} \end{cases}, \tag{7}$$

where subscripts q and d denote quadrature and direct axes, respectively; R_{rf} and L_{rf} are the resistance and inductance of the RSC filter, respectively; ω_1 is system angular line frequency; S_{rd} and S_{rq} denote RSC input switching signals; u_{dc} denotes the voltage across the DC-link capacitor (C_{dc}); u_s, i_s, L_s, and R_s are stator voltage, current, inductance, and resistance, respectively; u_g, i_g, L_{gf}, and R_{gf} are GSC filter voltage, current, inductance, and resistance, respectively; u_{sc} denotes the voltage across the compensation capacitor (C_{sc}); u denotes the voltage at the PCC; i denotes the current of the transmissions; e is the grid voltage; L_L and R_L are transmission inductance and resistance, respectively.

The system is expressed as follows:

$$\begin{cases} \dfrac{\mathrm{d}}{\mathrm{d}t}\boldsymbol{x} = \boldsymbol{f}(\boldsymbol{x}) + \boldsymbol{g}(\boldsymbol{x})\boldsymbol{u} \\ \boldsymbol{y} = \boldsymbol{h}(\boldsymbol{x}) \end{cases}, \tag{8}$$

where $\boldsymbol{u} = \begin{bmatrix} S_{rq} & S_{rd} \end{bmatrix}^T$; $\boldsymbol{y} = \begin{bmatrix} i_{rq} & i_{rd} \end{bmatrix}^T$; $\boldsymbol{x} = \begin{bmatrix} i_{rq} & i_{rd} & u_{dc} & i_{sq} & i_{sd} & i_{gq} & i_{gd} & i_q & i_d & u_{scq} & u_{scd} & \omega_m & \omega_r & \gamma \end{bmatrix}^T$. The expressions of $\boldsymbol{f}(\boldsymbol{x})$ and $\boldsymbol{g}(\boldsymbol{x})$ are given in the Appendix.

III. Feedback Linearization of DFIG-based WPP

System feedback linearizability is determined by relative degree, which depends on system outputs. The following condition should be fulfilled:

$$L_{\boldsymbol{g}} L_{\boldsymbol{f}}^{r_i - 1} h_i(\boldsymbol{x}) \neq 0, \tag{9}$$

where $h_i(\boldsymbol{x})$ is the system ith output; r_i denotes relative degree; L denotes a Lie derivative. Condition (9) should be fulfilled for both outputs. Thus, we can calculate the following:

$$\begin{cases} L_{g_1} L_{\boldsymbol{f}}^{1-1} h_1(\boldsymbol{x}) = L_{g_1} h_1(\boldsymbol{x}) = \dfrac{u_{dc}}{L_{rf}} S_{rq} \\ L_{g_2} L_{\boldsymbol{f}}^{1-1} h_1(\boldsymbol{x}) = L_{g_2} h_1(\boldsymbol{x}) = 0 \end{cases}, \tag{10}$$

$$\begin{cases} L_{g_1} L_{\boldsymbol{f}}^{1-1} h_2(\boldsymbol{x}) = L_{g_1} h_2(\boldsymbol{x}) = 0 \\ L_{g_2} L_{\boldsymbol{f}}^{1-1} h_2(\boldsymbol{x}) = L_{g_2} h_2(\boldsymbol{x}) = \dfrac{u_{dc}}{L_{rf}} S_{rd} \end{cases}. \tag{11}$$

The calculations expressed by Eqs. (10) and (11) demonstrate that the matrix is nonsingular.

$$\begin{bmatrix} L_{g_1} L_{\boldsymbol{f}}^{1-1} h_1(\boldsymbol{x}) & L_{g_2} L_{\boldsymbol{f}}^{1-1} h_1(\boldsymbol{x}) \\ L_{g_1} L_{\boldsymbol{f}}^{1-1} h_2(\boldsymbol{x}) & L_{g_2} L_{\boldsymbol{f}}^{1-1} h_2(\boldsymbol{x}) \end{bmatrix}$$

The relative degree is $r = r_1 + r_2 = 2 < 14$, indicating that the system can be partially linearized [26]. The system is devided into two subsystems as follows:

$$\frac{\mathrm{d}}{\mathrm{d}t}\tilde{\boldsymbol{z}} = \tilde{\boldsymbol{A}}\tilde{\boldsymbol{z}} + \tilde{\boldsymbol{B}}\tilde{\boldsymbol{v}}, \tag{12}$$

$$\frac{\mathrm{d}}{\mathrm{d}t}\hat{\boldsymbol{z}} = \hat{\boldsymbol{A}}\hat{\boldsymbol{z}}, \tag{13}$$

where $\tilde{\boldsymbol{z}}$ represents new states; $\hat{\boldsymbol{z}}$ represents the remaining states. The system states are as follows:

$$\boldsymbol{z} = \begin{bmatrix} \tilde{\boldsymbol{z}} & \hat{\boldsymbol{z}} \end{bmatrix}^T. \tag{14}$$

We choose coordinate transformation as follows

$$\begin{cases} \tilde{z}_1 = i_{rq} \\ \tilde{z}_2 = i_{rd} \end{cases}. \tag{15}$$

Then, we obtain the following:

$$\begin{cases} \dfrac{\mathrm{d}}{\mathrm{d}t}\tilde{z}_1 = \dfrac{\partial h_1(\boldsymbol{x})}{\partial \tilde{\boldsymbol{x}}} \dfrac{\mathrm{d}}{\mathrm{d}t}\boldsymbol{x} = -\omega_1 i_{rd} - \dfrac{R_{rf}}{L_{rf}} i_{rq} - \dfrac{u_{rq}}{L_{rf}} + \dfrac{u_{dc}}{L_{rf}} u_1 \\ \dfrac{\mathrm{d}}{\mathrm{d}t}\tilde{z}_2 = \dfrac{\partial h_2(\boldsymbol{x})}{\partial \tilde{\boldsymbol{x}}} \dfrac{\mathrm{d}}{\mathrm{d}t}\boldsymbol{x} = \omega_1 i_{rq} - \dfrac{R_{rf}}{L_{rf}} i_{rd} - \dfrac{u_{rd}}{L_{rf}} + \dfrac{u_{dc}}{L_{rf}} u_2 \end{cases}. \tag{16}$$

The linearized system is obtained with the use of the linear control method as $d\tilde{z}_i / dt = v_i$;

$$\begin{cases} v_1 = -\omega_1 i_{rd} - \dfrac{R_{rf}}{L_{rf}} i_{rq} - \dfrac{u_{rq}}{L_{rf}} + \dfrac{u_{dc}}{L_{rf}} u_1 \\ v_2 = \omega_1 i_{rq} - \dfrac{R_{rf}}{L_{rf}} i_{rd} - \dfrac{u_{rd}}{L_{rf}} + \dfrac{u_{dc}}{L_{rf}} u_2 \end{cases}, \tag{17}$$

where $\boldsymbol{v}$ is the input for linear control. Physical control laws are computed from Eq. (17) as follows:

$$\begin{cases} u_1 = \dfrac{L_{rf}}{u_{dc}} \left(v_1 + \omega_1 i_{rd} + \dfrac{R_{rf}}{L_{rf}} i_{rq} + \dfrac{u_{rq}}{L_{rf}} \right) \\ u_2 = \dfrac{L_{rf}}{u_{dc}} \left(v_2 - \omega_1 i_{rq} + \dfrac{R_{rf}}{L_{rf}} i_{rd} + \dfrac{u_{rd}}{L_{rf}} \right) \end{cases}. \tag{18}$$

The stability of the untransformed subsystem is ensured using zero-dynamic theory [9].

IV. SMC Design based on FL Model

A. Damping Controller Design

Sliding mode control is used based on the linearized system to improve robustness. The sliding mode surfaces are defined as follows:

$$\boldsymbol{S} = \begin{bmatrix} S_1 \\ S_2 \end{bmatrix} = \begin{bmatrix} e_1 + c_1 \int e_1 \\ e_2 + c_2 \int e_2 \end{bmatrix}, \tag{19}$$

where $e_1 = i_{rq} - i_{rq}^*$ and $e_2 = i_{rd} - i_{rd}^*$; c_1 and c_2 are positive constants. Reference values i_{rd}^* and i_{rq}^* are computed from reference rotor reactive power Q_r^* and active power P_r^* as follows:

$$\begin{cases} i_{rq}^* = \left(2P_r^*\right) / \left(3u_{rq}\right) \\ i_{rd}^* = \left(2Q_r^*\right) / \left(3u_{rd}\right) \end{cases}. \tag{20}$$

The equivalent control is derived in the solution of $\dot{\boldsymbol{S}}(t) = 0$ as follows:

$$\begin{cases} v_{1eq} = -c_1 e_1 \\ v_{2eq} = -c_2 e_2 \end{cases}. \tag{21}$$

The reaching control is added to the equivalent control as follows:

$$\begin{cases} v_1 = -k_1 S_1 - \varepsilon_1 \operatorname{sgn} S_1 - c_1 e_1 \\ v_2 = -k_2 S_2 - \varepsilon_2 \operatorname{sgn} S_2 - c_2 e_2 \end{cases}, \tag{22}$$

where ε_1, ε_2, k_1, and k_2 are positive parameters. A Lyapunov function is selected as follows:

$$V = \frac{1}{2} \boldsymbol{S}^T \boldsymbol{S} . \tag{23}$$

The time derivative of Eq. (23) is calculated as follows:

$$\begin{aligned} \dot{V} &= \boldsymbol{S}^T \dot{\boldsymbol{S}} = S_1 \left(\dot{e}_1 + c_1 e_1 \right) + S_2 \left(\dot{e}_2 + c_2 e_2 \right) \\ &= S_1 \left(-c_1 e_1 - \varepsilon_1 \operatorname{sgn} S_1 - k_1 S_1 + c_1 e_1 \right) \\ &\quad + S_2 \left(-c_2 e_2 - \varepsilon_2 \operatorname{sgn} S_2 - k_2 S_2 + c_2 e_2 \right) \\ &= -\varepsilon_1 \left| S_1 \right| - k_1 S_1^2 - \varepsilon_2 \left| S_2 \right| - k_2 S_2^2 < 0 \end{aligned} . \tag{24}$$

Hence, the designed control method is stable. With the substitution of Eq. (22) into Eq. (18), the control law is derived as follows:

$$\begin{cases} u_1 = \dfrac{L_{rf}}{u_{dc}} \left(\omega_1 i_{rd} + \dfrac{R_{rf}}{L_{rf}} i_{rq} + \dfrac{u_{rq}}{L_{rf}} - c_1 e_1 - \varepsilon_1 \operatorname{sgn} S_1 - k_1 S_1 \right) \\ u_2 = \dfrac{L_{rf}}{u_{dc}} \left(-\omega_1 i_{rq} + \dfrac{R_{rf}}{L_{rf}} i_{rd} + \dfrac{u_{rd}}{L_{rf}} - c_2 e_2 - \varepsilon_2 \operatorname{sgn} S_2 - k_2 S_2 \right) \end{cases} . \tag{25}$$

B. Parameter Tuning with PSO

Trial-and-error method is commonly used to determine SMC parameters [27]. For superior transient and steady-state performance, evolutionary algorithms, such as PSO and genetic algorithm (GA), are applied for SMC parameter tuning [28]. The advantages of PSO over other evolutionary techniques, such as GA, are as follows.

- Its implementation is easier.
- It requires less parameter tuning.
- It has higher memory ability than GA, and it is cheap in terms of computation time.

Therefore, PSO is used for FLSMC parameter tuning through the following procedure.

1) Initialization: The proposed damping controller has six control gains (c_1, c_2, ε_1, ε_2, k_1, and k_2); therefore, six particle positions are generated randomly as follows:

$$\begin{aligned} & x_{i,j}(0) = X_{i0} * \left[1 \pm \frac{5}{100} * rand(1,1) \right], \\ & i = 1,2,...,100,\ j = 1,2,...,6 \end{aligned} \tag{26}$$

where $x_{i,j}$ is the position of the jth particle in the ith group, and X_{i0} is the original value.

The velocity for position updating is expressed as follows:

$$\begin{cases} v_{j,\max} = \dfrac{x_{j,\max} - x_{j,\min}}{N} \\ v_{j,\min} = -v_{j,\max} \end{cases}, \tag{27}$$

where $v_{j,\min}$ and $v_{j,\max}$ are minimum and maximum velocities, respectively, of member j of the particles; $x_{j,\min}$ and $x_{j,\max}$ are the lower and upper bounds, respectively; N represents the dimension interval. Initial velocity is generated between $v_{j,\min}$ and $v_{j,\max}$. Other parameters are determined as follows:

$$\begin{cases} w_i = 0.9,\ w_f = 0.2 \\ \alpha = 0.98 \\ a_1 = 2,\ a_2 = 2 \end{cases}, \tag{28}$$

where w_i and w_f denote initial and final weights, respectively; α is the decay constant; a denotes the accelerating constant.

2) Evaluating Best Solution and Updating: The fitness value, which is expressed as follows, is assessed:

$$F = \max \left\{ \operatorname{Real}(\lambda_l), l = 1,2,...,14 \right\}, \tag{29}$$

where F denotes the fitness value, and λ_l denotes the system eigenvalues. The optimization objective is to drive all eigenvalues to the left half plane. The individual best solution is updated after each iteration.

3) Velocity and Position Updating: Velocity and position updating is expressed as follows:

$$\begin{aligned} v_{i,j}(t+1) = w(t) * v_{i,j}(t) + a_1 r_1 \left(x^* - x_{i,j}(t) \right) \\ + a_2 r_2 \left(x^{**} - x_{i,j}(t) \right) \end{aligned}, \tag{30}$$

$$x_{i,j}(t+1) = x_{i,j}(t) + v_{i,j}(t+1), \tag{31}$$

where r_1 and r_2 are uniformly distributed random numbers within [0, 1]; x^* and x^{**} represent individual and global best solutions, respectively.

4) Stopping Criteria: The search will stop if one of the following criteria is fulfilled. (i) The fitness value of the global best solution becomes smaller than a specified number, or (ii) the time counter is greater than the specified maximum number. Otherwise, the system will continue iterating until Step 2. The controller gains are presented in the Appendix.

V. Simulation Results and Analysis

A diagram of the proposed control method is presented in Fig. 2. SSRDC [8] and a PI controller [10], whose diagrams are presented in Figs. 3 and 4, respectively, are used for comparison. The parameters are presented in the Appendix.

A. Eigenvalue Analysis

The system eigenvalues are computed using the MATLAB function "linmod" [7]. System eigenvalues at different compensation levels, wind speeds, and number of online WTs are shown in Fig. 5. The figure shows that the FLSMC and SSRDC improve the capability of DFIGs in damping SSCI, and the capability of the proposed controller is better. Moreover, the proposed FLSMC stabilizes the studied system under varied operating conditions.

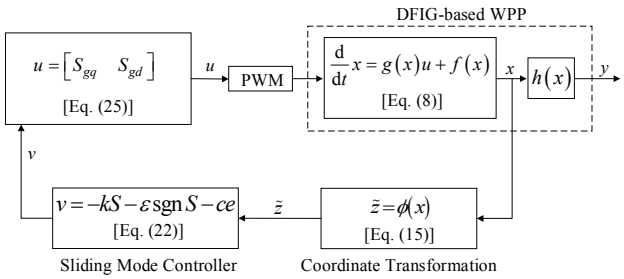

Fig. 2. Diagram of the FLSMC.

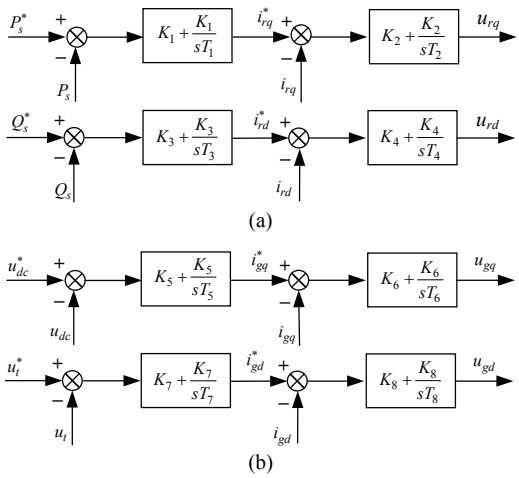

Fig. 3. PI controller: (a) RSC. (b) GSC.

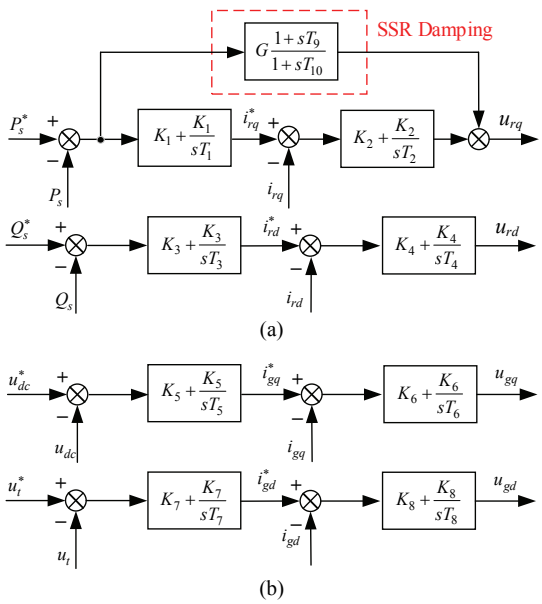

Fig. 4. SSRDC. (a) RSC. (b) GSC.

As presented in Fig. 5, a negative correlation exists between system damping and compensation level, whereas system damping has a positive correlation with wind speed. The number of online WTs has a nonlinear impact on SSCI, especially using PI controller and SSRDC. At a given wind speed and compensation level, a certain number of online WTs, which can cause severe damping, exists. However, system

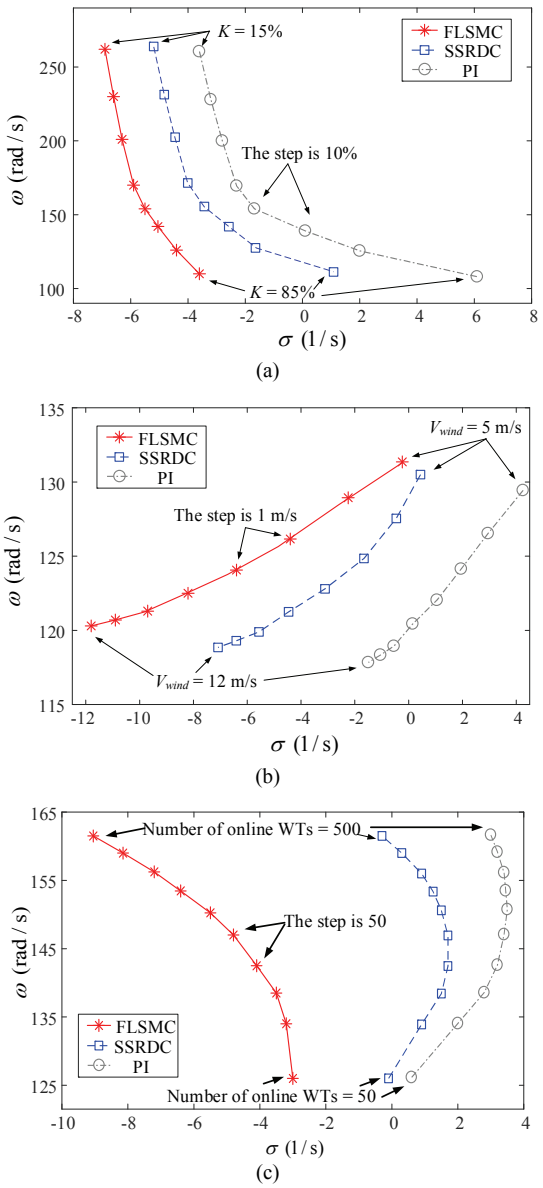

Fig. 5. System eigenvalues. (a) At varied compensation levels. (b) At varied wind speeds. (c) At varied number of online WTs.

damping generally improves with increased online WTs when FLSMC is used. This characteristic guarantees that the system stability will not be undermined with the incorporation of additional WTs in the future, once the system stability is ensured in the early-stage construction of WPP. In terms of WPP planning and practical power systems, this property of the FLSMC has major significance.

B. Electromagnetic Transient Simulation

In this section, the performance of the proposed FLSMC is evaluated using EMT simulation. Series compensation of 75% is provided to the transmissions at $t=1$ s with 7 m/s wind speed. Responses from the DFIG-based WPP are presented, including PCC voltage, active power of transmissions, and DC-link voltage.

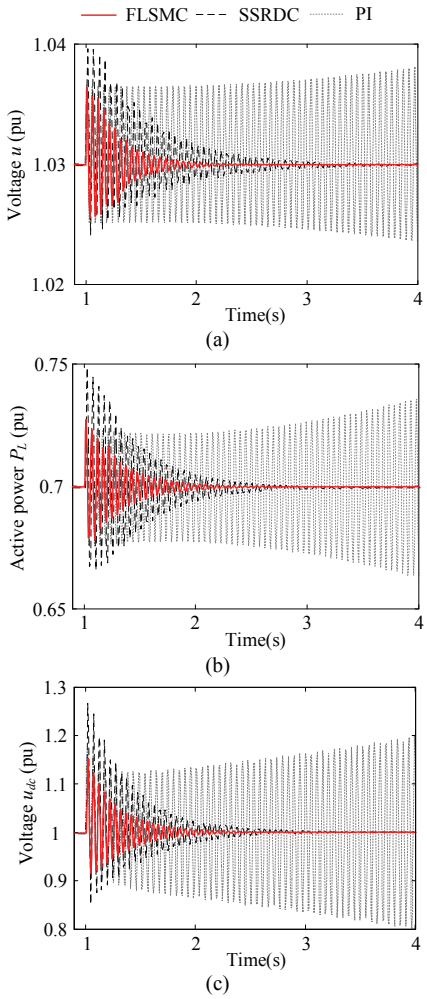

Fig. 6. DFIG responses for wind speed of 7 m/s and compensation level of 75%. (a) PCC voltage. (b) Transmission line active power; (c) DC-link voltage.

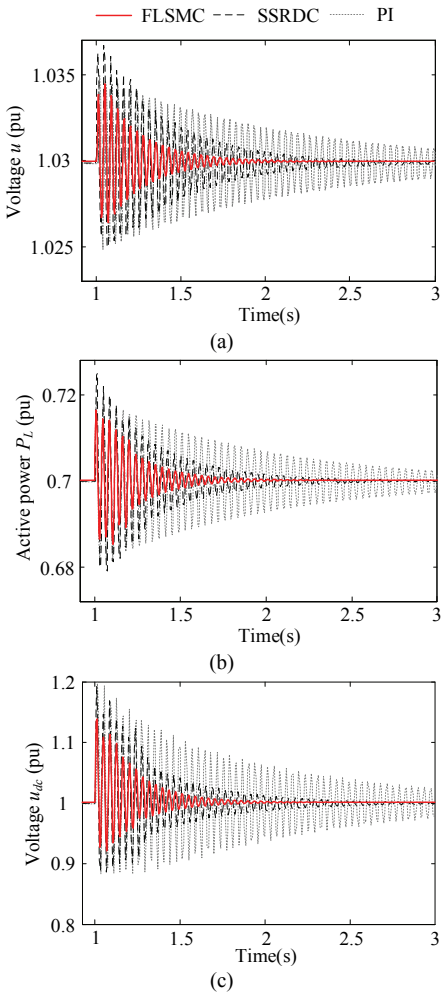

Fig. 7. DFIG responses for wind speed of 7 m/s and compensation level of 45%. (a) PCC voltage. (b) Transmission line active power. (c) DC-link voltage.

In Figs. 6(a) and 6(b), the presented waveforms show the effectiveness of the FLSMC and SSRDC in mitigating SSCI. Furthermore, the designed FLSMC exhibits superior damping performance; it consumes less time than does SSRDC to damp SSCI. In addition, Fig. 6(c) demonstrates the capability of the proposed FLSMC in damping fluctuations of the DC-link voltage. Given the proposed control laws, which are two nonlinear equations calculated online, the simulations require slightly higher CPU time to complete for FLSMC compared with the PI controller and SSRDC.

As presented in Fig. 7, the simulation is performed at 45% series compensation, whereas Fig. 8 demonstrates system responses at 9 m/s wind speed. In addition to the better damping capability of the proposed FLSMC, transient SSCI problems are observed to be less severe at lower compensation levels or higher wind speeds.

In practice, DFIG parameters vary to a certain extent. The variations of the rotor resistance (R_r), stator resistance (R_s), stator leakage inductance (L_{ls}), rotor leakage inductance (L_{lr}), and mutual inductance (L_m) could influence the characteristics of the SSCI [3]. However, at the frequencies in this study, the impedances of the inductance (L_{ls}, L_{lr}, and L_m) are much larger than those of the resistances (R_r, R_s), i.e., $j\omega L >> R$. Thus, the analysis mainly focuses on the impact from the variations of the inductance (L_{ls}, L_{lr}, and L_m). When SSCI occurs, the increasing saturation degree of the leakage flux and main flux leads to decreases in the values of L_{ls}, L_{lr}, and L_m [8], [29]. Fig. 9 presents the simulation results at 75% series compensation and 7 m/s wind speed with L_{ls}, L_{lr}, and L_m reduced to 80% of the nominal value. As shown in Fig. 9, the SSRDC can still damp oscillations. However, more than 4 s is required for the SSRDC to eliminate the SSCI, much longer compared with that shown in Fig. 6. Moreover, due to parameter variations, the fluctuation range of DC-link voltage is larger with SSRDC. On the contrary, the performance of the FLSMC is not much affected by DFIG parameter deviation. Although the fluctuations in system responses increase slightly, FLSMC is still capable of mitigating SSCI within 3 s. The simulation results demonstrate the strong robustness of the proposed controller against parameter variations.

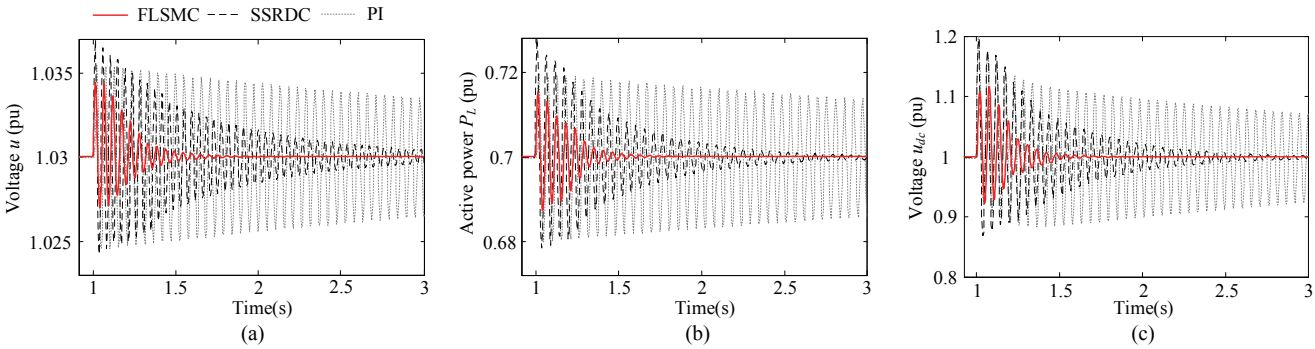

Fig. 8. DFIG responses for wind speed of 9 m/s and compensation level of 75%. (a) PCC voltage. (b) Transmission line active power. (c) DC-link voltage.

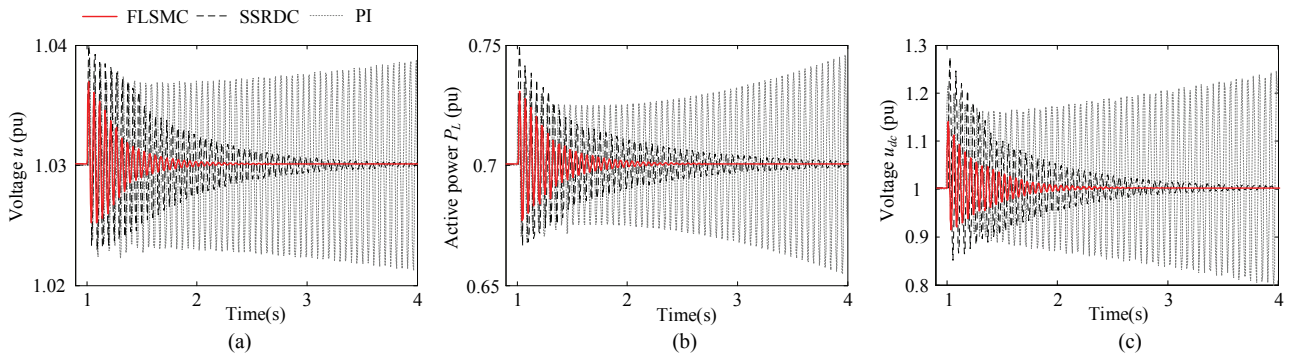

Fig. 9. DFIG responses under parameter variations for wind speed of 7 m/s and compensation level of 75%. (a) PCC voltage. (b) Transmission line active power. (c) DC-link voltage.

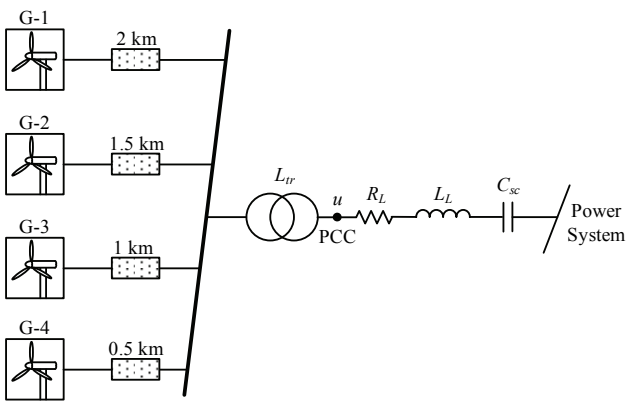

Fig. 10. Series-compensated WPP with collector cable.

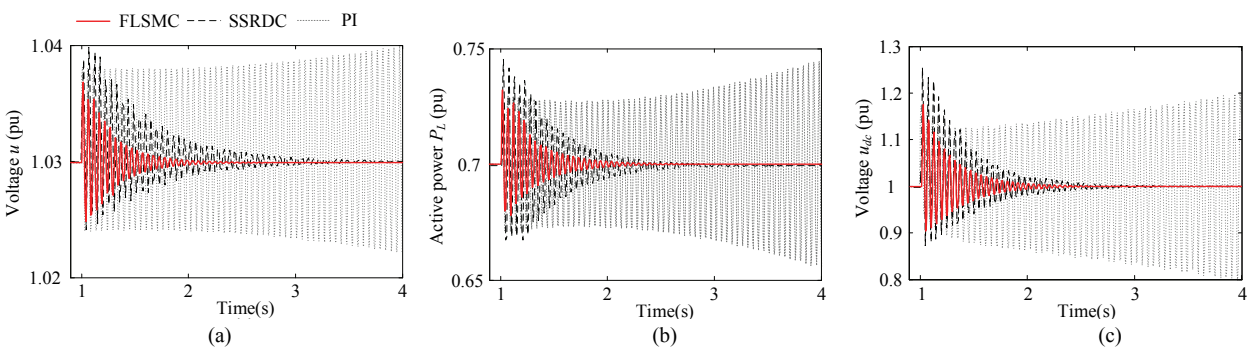

Fig. 11. DFIG responses based on realistic WPP for wind speed of 7 m/s and compensation level of 75%. (a) PCC voltage. (b) Transmission line active power. (c) DC-link voltage.

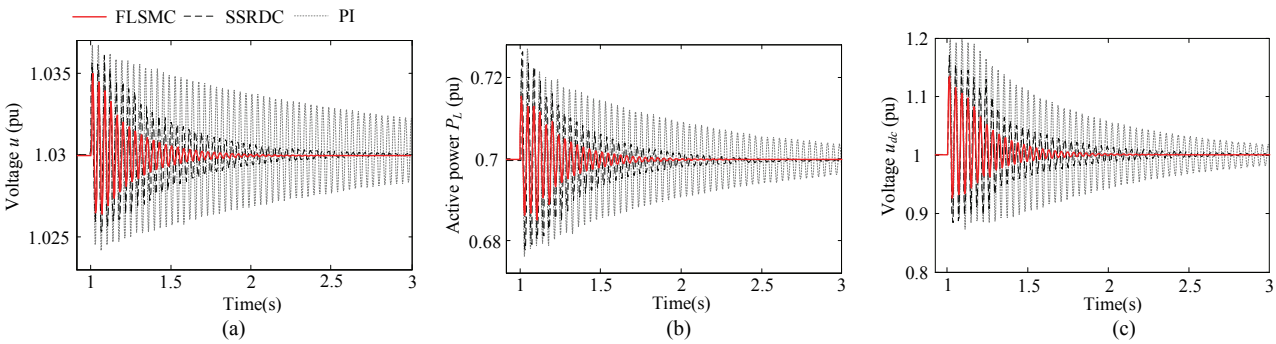

Fig. 12. DFIG responses based on realistic WPP for wind speed of 7 m/s and compensation level of 45%. (a) PCC voltage. (b) Transmission line active power. (c) DC-link voltage.

We present the potential of SSCI in a realistic DFIG WPP divided into different groups connected by cables, as illustrated in Fig. 10. The WPP is divided into four groups (G-1 to G-4). Each group is composed of 20 wind turbine generators (WTGs), and all groups are linked to PCC via collector cables. G1 and G2 consist of WTG-1, each rated 2 MW; G3 and G4 consist of WTG-2, each rated 2.3 MW. WTG-1 is used in this analysis, and the parameters of WTG-2 are provided in the Appendix. The cable length varies between 0.5 and 2 km, as shown in Fig. 10 [30]. The layout of a realistic wind farm is presented in detail in [31]. EMT simulation is performed under different wind power output conditions. In this case, G-1, G-2, G-3, and G-4 produce 100%, 75%, 50%, and 25% of their rated capacity, respectively. Series compensation of 75% is given to the transmission line at $t = 1$ s. Responses from the DFIG-based WPP are presented in Fig. 11. As shown in Fig. 11, the WPP with the PI controller has SSCI. On the contrary, oscillations are damped with SSRDC and FLSMC. Moreover, less time is required to completely eliminate SSCI under the proposed FLSMC. The simulation is repeated at the series compensation of 45%, as illustrated in Fig. 12. The damping performance of FLSMC is superior to that of the PI controller and SSRDC.

VI. Conclusion

SSCI is caused by the interaction of DFIG-based WPPs with series compensation. Thus, a robust nonlinear controller is designed in this work using feedback linearization and sliding mode control to mitigate SSCI in consideration of the parameter variations and inherent nonlinearities of DFIGs. FLSMC is developed for RSC through feedback linearization, design of the sliding mode controller, and parameter tuning with use of PSO. The performance of the FLSMC is assessed and compared with that of the PI controller and SSRDC. Eigenvalue analysis is performed under varied operating conditions. With regard to the superior capability of FLSMC in alleviating SSCI, (i) system damping deteriorates with decreased wind speed or increased compensation levels, and (ii) the number of online WTs has a nonlinear impact on SSCI damping. EMT simulation is subsequently carried out to validate eigenvalue analysis. EMT simulation results show that the designed FLSMC enhances SSCI damping and robustness properties of the studied system.

Appendix

TABLE I
System Parameters

Parameter	Value
Stator resistance (R_s)	0.0084 p.u.
Stator inductance (L_s)	0.1670 p.u.
RSC filter resistance (R_{rf})	0.0083 p.u.
RSC filter inductance (L_{rf})	0.1323 p.u.
GSC filter resistance (R_{gf})	0.0015 p.u.
GSC filter inductance (L_{gf})	0.1500 p.u.
DC-link capacitance (C_{dc})	10 mF
Generator damping coefficient (D_g)	0.5 p.u.
Turbine damping coefficient (D_t)	2.5 p.u.
Generator inertia constant (H_g)	0.5 p.u.
Turbine inertia constant (H_t)	2.5 p.u.
Transmission line resistance (R_L)	0.02 p.u.
Transmission line inductance (L_L)	0.0016 p.u.

TABLE II
Parameters of WTG-2

Parameter	Value
Stator resistance	0.0051 p.u.
Stator inductance	0.1317 p.u.
RSC filter resistance (R_{rf})	0.0112 p.u.
RSC filter inductance (L_{rf})	0 p.u.
GSC filter resistance (R_{gf})	0.1924 p.u.
GSC filter inductance (L_{gf})	0.2117 p.u.
Generator damping coefficient (D_g)	0 p.u.
Turbine damping coefficient (D_t)	0.3 p.u.
Generator inertia constant (H_g)	0.5 p.u.
Turbine inertia constant (H_t)	4 p.u.

TABLE III
CONTROLLER GAINS

Parameter	Value	Parameter	Value
K_1	0.0001	T_1	0.0500
K_2	0.0000	T_2	0.0050
K_3	0.0001	T_3	0.0250
K_4	0.0001	T_4	0.0025
K_5	0.1000	T_5	0.0500
K_6	1	T_6	100
K_7	0.1000	T_7	0.0500
K_8	1	T_8	100
G	30	T_9	0.0500
k_1	100	T_{10}	100
k_2	200	c_1	200
ε_1	1	c_2	500
ε_2	0.5		

Expressions of $\boldsymbol{g}(\boldsymbol{x})$ *and* $\boldsymbol{f}(\boldsymbol{x})$

$$\boldsymbol{g}(\boldsymbol{x})=\begin{bmatrix} \frac{u_{dc}}{L_{rf}} & 0 \\ 0 & \frac{u_{dc}}{L_{rf}} \\ -\frac{1}{C_{dc}}i_{rq} & -\frac{1}{C_{dc}}i_{rd} \\ 0 & 0 \\ 0 & 0 \\ 0 & 0 \\ 0 & 0 \\ 0 & 0 \\ 0 & 0 \\ 0 & 0 \\ 0 & 0 \\ 0 & 0 \\ 0 & 0 \\ 0 & 0 \end{bmatrix}$$

$$\boldsymbol{f}(\boldsymbol{x})=\begin{bmatrix} -\omega_1 i_{rd}-\frac{R_{rf}}{L_{rf}}i_{rq}-\frac{u_{rq}}{L_{rf}} \\ \omega_1 i_{rq}-\frac{R_{rf}}{L_{rf}}i_{rd}-\frac{u_{rd}}{L_{rf}} \\ \frac{i_{dc}}{C_{dc}} \\ -\omega_1 i_{sd}+\frac{R_s}{L_s}i_{sq}+\frac{u_{sq}}{L_s} \\ \omega_1 i_{sq}+\frac{R_s}{L_s}i_{sd}+\frac{u_{sd}}{L_s} \\ \omega_1 i_{gd}-\frac{u_{gq}}{L_{gf}}-\frac{R_{gf}}{L_{gf}}i_{gq} \\ -\omega_1 i_{gq}-\frac{u_{gd}}{L_{gf}}-\frac{R_{gf}}{L_{gf}}i_{gd} \\ -\omega_1 i_d+\frac{R_L}{L_L}i_q+\frac{1}{L_L}\left(u_q-u_{scq}-e_q\right) \\ \omega_1 i_q+\frac{R_L}{L_L}i_d+\frac{1}{L_L}\left(u_d-u_{scd}-e_d\right) \\ \frac{i_q}{C_{sc}}-\omega_1 u_{scd} \\ \frac{i_d}{C_{sc}}+\omega_1 u_{scq} \\ \frac{T_{ae}-D_t\omega_m-K_s\gamma}{2H_t} \\ \frac{K_s\gamma-D_g\omega_r-T_e}{2H_g} \\ 2\pi f\left(\omega_m-\frac{\omega_r}{N_g}\right) \end{bmatrix}$$

REFERENCES

[1] A. Moharana and R. K. Varma, "Subsynchronous resonance in single cage self-excited induction generator based wind farm connected to series-compensated lines," *IET Gener. Transm. Distrib.*, Vol. 5, No. 12, pp. 1221-1232, Dec. 2011.

[2] H. Cho, S. Oh, S. Nam, and B. Lee, "Non-linear dynamics based sub-synchronous resonance index by using power system measurement data," *IET Gener. Transm. Distrib.*, Vol. 12, No. 17, pp. 4026-4033, Sep. 2018.

[3] X. Xie, X. Zhang, H. Liu, H. Liu, Y. Li, and C. Zhang, "Characteristic analysis of subsynchronous resonance in practical wind farms connected to series-compensated transmissions," *IEEE Trans. Energy Convers.*, Vol. 32, No. 3, pp. 1117-1126, Sep. 2017.

[4] L. Xiong, P. Li, F. Wu, and J. Wang, "Stability enhancement of power systems with high DFIG-wind turbine penetration via virtual inertia planning," *IEEE Trans. Power Syst.*, to be published.

[5] V. B. Virulkar and G. V. Gotmare, "Sub-synchronous resonance in series compensated wind farm: A review," *Renew. Sustain. Energy Rev.*, Vol. 55, pp. 1010-1029, Mar. 2016.

[6] P. Li, J. Wang, L. Xiong, and F. Wu, "Nonlinear controllers based on exact feedback linearization for series-compensated DFIG-based wind parks to mitigate sub-synchronous control interaction," *Energies*, Vol. 10, No. 8, pp. 1182, Aug. 2017.

[7] P. Li, L. Xiong, F. Wu, M. Ma, and J. Wang, "Sliding mode controller based on feedback linearization for damping of sub-synchronous control interaction in DFIG-based wind power plants," *Int. J. Electr. Power Energy Syst.*, Vol. 107, pp. 239-250, May 2019.

[8] G. Irwin, A. Jindal, and A. Isaacs, "Sub-synchronous control interactions between type 3 wind turbines and series compensated ac transmission systems," in *Proc. IEEE Power Energy Gen. Meet.*, pp. 1-6, Jul. 2011.

[9] P. Li, J. Wang, F. Wu, and H. Li. "Nonlinear controller based on state feedback linearization for series-compensated DFIG-based wind power plants to mitigate sub-synchronous control interaction," *Int. Trans. Electr. Energ. Syst.*, e2682, 2018.

[10] H. A. Mohammadpour and E. Santi, "Modeling and control of gate-controlled series capacitor interfaced with a DFIG-based wind farm," *IEEE Trans. Ind. Electron.*, Vol. 62, No. 2, pp. 1022-1033, Feb. 2015.

[11] X. Zhu, M. Jin, X. Kong, J. Zhao, J. Liu, and Q. Zhou, "Subsynchronous resonance and its mitigation for power system with unified power flow controller," *J. Mod. Power Syst. Clean Energy*, Vol. 6, No. 1, pp. 181-189, Jan. 2018.
[12] S. Wang, S. Lu, H. Xiao, Z. Xu, X. Cui, and X. Wu, "SSO suppression method and effectiveness of STATCOM in an identical multi-machine system," *J. Engineering*, Vol. 2017, No. 13, pp. 1483-1487, Oct. 2017.
[13] R. Zheng, T. Joseph, S. Wang, and J. Liang, "A control strategy for TCSC to mitigate SSR with local measurements," *IET International Conference on AD and DC Power Transmission*, pp. 1-6, 2017.
[14] X. Xie, H. Liu, and Y. Han, "Coordinated design of supplementary excitation damping controller and voltage-sourced converter based generator terminal subsynchronous damping controller for subsynchronous resonance suppression: a case study," *Electr. Power Components Syst.*, Vol. 44, No. 5, pp. 565-577, Feb. 2016.
[15] M. R. Qader, "Fuzzy control strategy for camping sub-synchronous resonance," *J. Electr. Eng. Technol.*, Vol. 13, No. 5, pp. 1791-1797, Sep. 2018.
[16] J. Taherahmadi, M. Jafarian, and M. N. Asefi, "Using adaptive control in DFIG-based wind turbines to improve the subsynchronous oscillations of nearby synchronous generators," *IET Renew. Power Gener.*, Vol. 11, No. 2, pp. 362-369, Apr. 2017.
[17] R. Mahalakshmi and K. C. S. Thampatty, "A fuzzy based adaptive controller for grid connected DFIG based windfarm for damping SSR oscillations," *TENCON 2017 IEEE Reg. Conf.*, pp. 2138-2143, 2017.
[18] F. Zhao F. Zhao, L. Wu, J. Zhang, X. Gao, H. Liu, H. Wang, and Y. Yang, "Suppression method of parallel-damping controller for DFIG," *J. Engineering*, Vol. 2017, No. 13, pp. 880-884, Oct. 2017.
[19] H. Liu, X. Xie, J. He, H. Liu, and Y. Li, "Damping DFIG-associated SSR by adding subsynchronous suppression filters to DFIG converter controllers," *IEEE Power Energy Soc. Gen. Meet.*, pp. 1-5, 2016.
[20] H. K. Nia, F. Salehi, M. Sahni, N. Karnik, and H. Yin, "A filter-less robust controller for damping SSCI oscillations in wind power plants," *IEEE Power Energy Soc. Gen. Meet.*, pp. 1-5, Jan. 2018.
[21] S. M. Mohiuddin, M. A. Mahmud, A. M. O. Haruni, and H. R. Pota, "Design and implementation of partial feedback linearizing controller for grid-connected fuel cell systems," *Int. J. Electr. Power Energy Syst.*, Vol. 93, pp. 414-425, Dec. 2017.
[22] L. Xiong, P. Li, H. Li, and J. Wang, "Sliding mode control of DFIG wind turbines with a fast exponential reaching law," *Energies*, Vol. 10, No. 11, 1788, Nov. 2017.
[23] L. Xiong, P. Li, F. Wu, M. Ma, M. W. Khan, and J. Wang, "A coordinated high-order sliding mode control of DFIG wind turbine for power optimization and grid synchronization," *Int. J. Electr. Power Energy Syst.*, Vol. 105, pp. 679-689, Feb. 2019.
[24] L. Xiong, J. Wang, X. Mi, and W. Khan, "Fractional order sliding mode based direct power control of grid-connected DFIG," *IEEE Trans. Power Syst.*, Vol. 33, No. 3, pp. 3087-3096, May. 2018.
[25] P. Li, J. Wang, L. Xiong, and M. Ma, "Robust nonlinear controller design for damping of sub-synchronous control interaction in DFIG-based wind farms," *IEEE Access*, to be published.
[26] M. A. Mahmud, H. R. Pota, and M. J. Hossain, "Dynamic stability of three-phase grid-connected photovoltaic system using zero dynamic design approach," *IEEE J. Photovoltaics*, Vol. 2, No. 4, pp. 564-571, Oct. 2012.
[27] M. Han, J. Fan, and J. Wang, "A dynamic feedforward neural network based on gaussian particle swarm optimization and its application for predictive control," *IEEE Trans. Neural Networks*, Vol. 22, No. 9, pp. 1457-1468, Sep. 2011.
[28] P. Siano and G. Mokryani, "Assessing wind turbines placement in a distribution market environment by using particle swarm optimization," *IEEE Trans. Power Syst.*, Vol. 28, No. 4, pp. 3852-3864, Nov. 2013.
[29] H. M. Jabr and N. C. Kar, "Effects of main and leakage flux saturation on the transient performances of doubly-fed wind driven induction generator," *Electr. Power Syst. Res.*, Vol. 77, No. 8, pp. 1019-1027, Jun. 2007.
[30] R. K. Varma and A. Moharana, "SSR in double-cage induction generator-based wind farm connected to series-compensated transmission line," *IEEE Trans. Power Syst.*, Vol. 28, No. 3, pp. 2573-2583, Aug. 2013.
[31] S. Liang, Q. Hu, W. Lee, "A survey of harmonic emissions of a commercially operated wind farm," *IEEE Trans. Ind. Appl.*, Vol. 48, No. 3, pp. 1115-1123, May 2015.

Penghan Li was born in Shanxi, China, in 1993. He received his B.S. degree in Electrical Engineering from Harbin Institute of Technology, Harbin, China, in 2016. He is working toward his Ph.D. degree in electrical engineering in the School of Electronic Information and Electrical Engineering at Shanghai Jiao Tong University, Shanghai, China. His research interests include power system nonlinear control, sub-synchronous interaction, and DFIG control.

Linyun Xiong was born in Chongqing, China, in 1993. He received his B.S. degree in Electrical Engineering from Sichuan University, Chengdu, China, in 2015. He is working toward his Ph.D. degree in the School of Electronic Information and Electrical Engineering at Shanghai Jiao Tong University, Shanghai, China. His research interests include power system nonlinear control and Hamiltonian systems.

Jie Wang was born in Jiangsu, China, in 1960. He received his M.S. degree from the North China Electric Power University, Baoding, China, in 1991, and his Ph.D. degree from Northeastern University, Shenyang, China, in 1998. From 1999 to 2001, he researched nonlinear control and Hamiltonian systems in Shanghai Jiao Tong University, Shanghai, China. From 1982 to 2002, he worked on industrial automation and power system automation. He is presently working in the field of power system stability and control.

Meiling Ma was born in Jiangsu, China, in 1991. She received her B.S. and M.S. degrees from Nanjing Normal University, Nanjing, China, in 2012 and 2015, respectively. From 2015 to 2017, she worked in the field of nonlinear dynamics of power systems in Nanjing Normal University Taizhou College, Taizhou, China. She is currently working toward her Ph.D. degree in the School of Electronic Information and Electrical Engineering at Shanghai Jiao Tong University, Shanghai, China. Her research interests include power system transient stability and Hamilton realization of power systems.

Muhammad Waseem Khan received his B.E. degree from the Department of Electrical Engineering, Sarhad University of Science and Information Technology, Peshawar, Pakistan, in 2012, and his M.S. degree from the Department of Electrical Engineering, Shanghai Jiao Tong University, Shanghai, China, in 2017. He is currently a Ph.D. research scholar in the Department of Electrical Engineering, Shanghai Jiao Tong University, Shanghai, China. His research interests include microgrid control, optimization, and management using multi-agent systems for the integration of distributed renewable energy generation.